LETTER

Interdependence of behavioural variability and response to small stimuli in bacteria

Heungwon Park[1], William Pontius[2], Calin C. Guet[3], John F. Marko[4], Thierry Emonet[2] & Philippe Cluzel[3]

The chemotaxis signalling network in *Escherichia coli* that controls the locomotion of bacteria is a classic model system for signal transduction[1,2]. This pathway modulates the behaviour of flagellar motors to propel bacteria towards sources of chemical attractants. Although this system relaxes to a steady state in response to environmental changes, the signalling events within the chemotaxis network are noisy and cause large temporal variations of the motor behaviour even in the absence of stimulus[3]. That the same signalling network governs both behavioural variability and cellular response raises the question of whether these two traits are independent. Here, we experimentally establish a fluctuation–response relationship in the chemotaxis system of living bacteria. Using this relationship, we demonstrate the possibility of inferring the cellular response from the behavioural variability measured before stimulus. In monitoring the pre- and post-stimulus switching behaviour of individual bacterial motors, we found that variability scales linearly with the response time for different functioning states of the cell. This study highlights that the fundamental relationship between fluctuation and response is not constrained to physical systems at thermodynamic equilibrium[4] but is extensible to living cells[5]. Such a relationship not only implies that behavioural variability and cellular response can be coupled traits, but it also provides a general framework within which we can examine how the selection of a network design shapes this interdependence.

It is standard procedure to characterize the stochastic dynamics of physical systems in thermodynamic equilibrium by measuring spontaneous fluctuations and responses to small external perturbations. Because these two distinct measurements contain the same information, they are related by the fluctuation-dissipation theorem[4]. Although the fluctuation-dissipation theorem has practical applications—to evaluate force-extension sensors for single biomolecules[6,7] and to predict static cell-to-cell variability of gene expression[8,9]—it has not been possible to apply it directly to the study of the dynamical behaviour of living cells because they are open systems with significant non-thermal dynamics. However, this theorem has recently been extended to a fluctuation-response theorem (FRT) for systems that are not in thermodynamic equilibrium but that have a well-defined steady state and Markovian dynamics[5,10–12]. For application to living cells this condition amounts to studying dynamic processes with sufficiently short 'memory' that they can relax to a well-defined steady state. Here we use the FRT as an operational framework to establish the interdependence of distinct cellular traits, such as cellular fluctuations and response to a small stimulus, without relying on the biochemical details of a specific signalling pathway. To tackle this question experimentally, we used the well-characterized chemotaxis system in *E. coli*, which governs bacterial locomotion[13].

The chemotaxis network regulates the rotation direction—clockwise (CW) or counter-clockwise (CCW)—of the flagellar motors, which control the swimming direction of the cell[1,2]. One of the hallmarks of

bacterial chemotaxis is adaptation. Following a stepwise stimulus, the CW bias (the probability that the motor will rotate clockwise) decreases abruptly, before slowly adapting back to its pre-stimulus level. Even when bacteria are adapted to their environment, the CW bias of individual cells fluctuates around the mean. These temporal fluctuations in CW bias reflect slow fluctuations in signalling events throughout the transduction network[14]. To verify that the bacterial chemotaxis system satisfies the FRT, we monitored both the temporal fluctuations of the CW bias before stimulus and the cellular response to a small stimulus at the single-cell level. Both quantities were obtained from the time series of CW and CCW intervals of individual motors from bacteria immobilized on a glass coverslip[15] and submerged in a motility medium that does not support growth. Such single-cell experiments are complicated by inherent cell-to-cell differences in relative chemotaxis protein concentration, leading to differences in switching dynamics (Fig. 1a). To compare cells with similar behaviour, we sorted wild-type cells according to their steady-state CW bias (Fig. 1a). These CW bias bins define different classes of cells, which, despite being genetically identical, have different dynamics and must be analysed separately[3].

First, we quantified the response in single cells by measuring the length of successive CCW intervals immediately following the stimulus. The stimulus (10 nM of aspartate) used in this study is small and close to the limit of sensitivity of the bacterial chemotaxis system[16]. At the single-cell level, the length of the first CCW interval following the small stimulus (Supplementary Fig. 1a) was distributed around the mean CCW interval length before stimulus (Supplementary Fig. 1b). Given that CCW interval length is a stochastic variable, we averaged the CCW interval lengths after stimulus between cells and found that the mean length of the first CCW interval following stimulus was slightly longer than the mean pre-stimulus CCW interval length (Fig. 1b). Therefore, we expected the response of the system to be within the linear regime, which was necessary to apply the FRT. We also tested the response of the chemotaxis system for a stimulus 100 times larger (1 μM aspartate). Surprisingly, the second CCW interval following the stimulus returned to near pre-stimulus length for both large and small attractant concentrations (Fig. 1c). Although the cellular response to stimulus extends in some cases beyond the second interval (Supplementary Fig. 1d, e), these results qualitatively indicate that the first CCW interval contains most of the chemotactic response to both small and large stimuli.

To characterize the system quantitatively, we defined the response time of a single cell as the cumulative length of post-stimulus CCW intervals that are strictly longer than the mean CCW interval length before stimulus (Fig. 1b, c and Supplementary Fig. 1e; see Methods for definition of response time). This procedure yields a reasonable estimate of the response time under the condition of small stimulus (Supplementary Fig. 2). We found that the response time averaged over CW bias bins decreased with CW bias for both small (Fig. 2a) and large stimuli (Fig. 2a, inset). Because all cells returned to their pre-stimulus behaviour

[1]The James Franck Institute, The Institute for Biophysical Dynamics, and The Department of Physics, University of Chicago, Chicago, Illinois 60637, USA. [2]Department of Molecular, Cellular, and Developmental Biology and Department of Physics, Yale University, New Haven, Connecticut 06520, USA. [3]FAS Center for Systems Biology, Department of Molecular and Cellular Biology, and School of Engineering and Applied Sciences, Harvard University, 52 Oxford Street, Cambridge, Massachusetts 02138, USA. [4]Department of Molecular Biosciences and Department of Physics and Astronomy, Northwestern University, Evanston, Illinois 60208, USA.
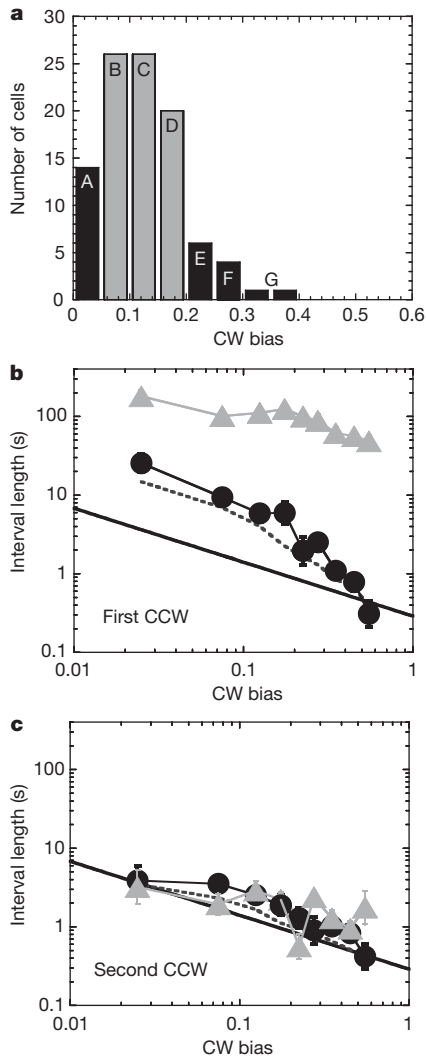
Figure 1 | CCW interval lengths pre- and post-stimulus. a, Histogram of CW bias of wild-type RP437 cells. We sorted cells into CW bias intervals by their pre-stimulus CW bias: 0.00–0.05 (A), 0.05–0.10 (B), 0.10–0.15 (C), 0.15–0.20 (D), 0.20–0.25 (E), 0.25–0.30 (F), 0.30–0.40 (G), 0.40–0.50 (H) and 0.50–0.60 (I). Grey bars are cells representative of wild-type behaviour. To increase the chance of obtaining cells with CW bias higher than 0.2, we transformed wild-type cells with pZE21-CheR (Methods). This extended the range of CW bias considered in our study to values greater than 0.4: bins H and I (not shown). **b, c**, The first (**b**) and second (**c**) mean post-stimulus CCW interval lengths versus pre-stimulus CW bias for all cells (wild-type RP437 and RP437 expressing CheR from pZE21-CheR). (See Supplementary Fig. 1 for individual cells.) Black circles, cells exposed to a small stimulus (10 nM L-aspartate). Grey triangles, cells exposed to a large stimulus (1 µM L-aspartate). Error bars show the standard error associated with the average CCW interval length in each bin. Dark grey dashed line, geometric mean of the CCW interval lengths following a randomly chosen time point in non-stimulated cells. Black line, power-law fit of the geometric mean of pre-stimulus CCW interval lengths calculated over 1,500 s for all cells (wild-type RP437 and RP437 expressing extra CheR from pZE21-CheR) as a function of the pre-stimulus CW bias (Supplementary Fig. 1b).

(Supplementary Fig. 1), the system exhibited near-precise adaptation at the single-cell level, regardless of CW bias (Supplementary Fig. 3). This result agrees with that obtained from population measurements[17,18] and shows that the dynamics have sufficiently short 'memory' and that individual cells can relax to a well-defined steady state.

A direct consequence of the linear approximation is that the response time of the system to a small external stimulus should be proportional to the correlation time of the spontaneous fluctuations before stimulus. Using serial correlation analysis[19,20], we evaluated
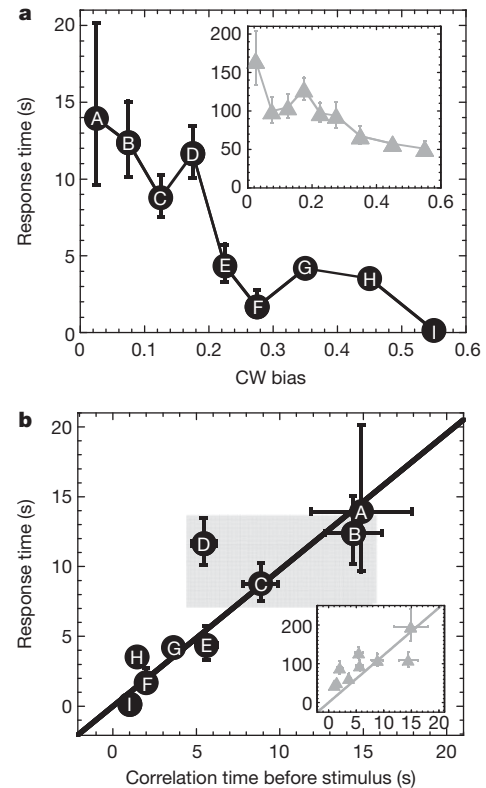

Figure 2 | Relationship between response to stimulus and fluctuations before stimulus. a, Average response time for all cells (wild-type RP437 and RP437 expressing extra CheR from pZE21-CheR) exposed to a stepwise small stimulus (black circles, 10 nM L-aspartate) or large stimulus (grey triangles in inset to **a**, 1 µM L-aspartate). The letters correspond to the CW bias bins (Fig. 1a). Error bars show the standard error associated with the average response time within each bin. **b**, Average response time to a small stimulus (black circles) or large stimulus (grey triangles in inset to **b**) as a function of the correlation time for all cells (wild-type RP437 and RP437 expressing CheR from pZE21-CheR). For the large stimulus, the average response time was adjusted by a correction factor (Supplementary Fig. 2c). The solid lines are linear fit functions forced through the origin. For the black line: response time = C × correlation time. C ≈ 0.98 ± 0.10 (R^2 = 0.75). For the grey line in the inset: relaxation time = C × correlation time. C ≈ 12.23 ± 1.83 (R^2 = 0.07). Error bars for the correlation time are the half-lengths of the first uncorrelated CCW intervals. Error bars for the response time are the standard error associated with the average response time within each bin. Grey area, representative behaviour of a wild-type population. Insets in **a** and **b** share axes with the main panels.

the correlation time in non-stimulated cells (Supplementary Fig. 4). In agreement with our assumption of linear dynamics[21] and the general prediction of the FRT, we found that the correlation time scales linearly with the response time to small stimulus (R^2 = 0.75; Fig. 2b) whereas to large stimulus it scales poorly (R^2 = 0.07; Fig. 2b, inset). This result has an important practical implication: The response time that governs the cellular response in chemotaxis can be experimentally inferred by measuring the temporal correlations in behavioural fluctuations from cells before stimulus.

Cellular behavioural variability can also be defined by the amplitude of the noise rather than its temporal correlations. To characterize the amplitude of the output noise of the chemotaxis network, we computed the power spectral density of the switching binary time series measured from individual motors before stimulus (Fig. 3a and Supplementary Fig. 5). We evaluated the low-frequency noise by integrating the power spectrum between $f = 1/1,500 \, \text{s}^{-1}$ and $f = 1/10 \, \text{s}^{-1}$. In this frequency range, the temporal fluctuations are putatively caused by the slow methylation–demethylation of the receptor-kinase complexes that are also controlling the adaptive process[14]. Two elements
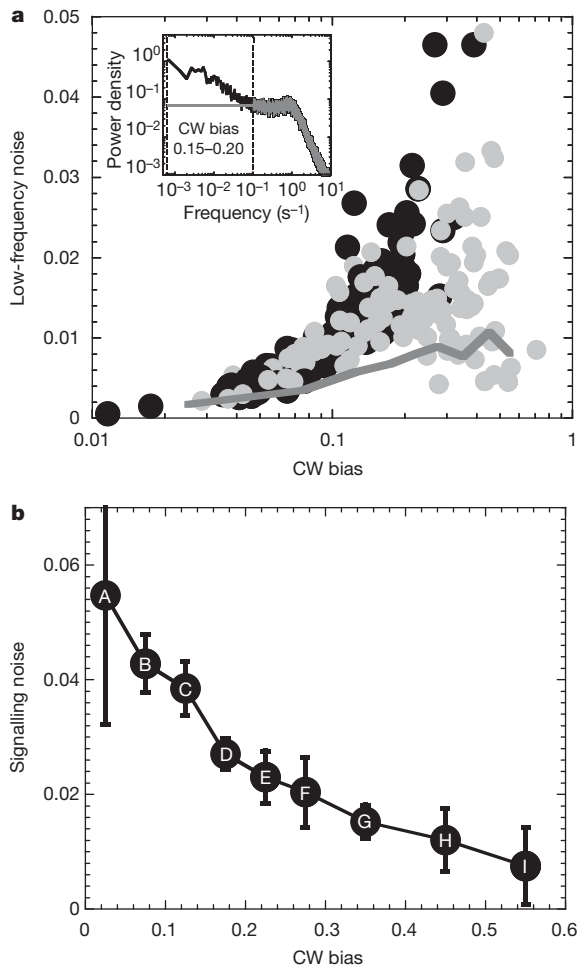
Figure 3 | Low-frequency noise in non-stimulated cells. a, Low-frequency noise in individual wild-type RP437 cells (black) and RP437 cells expressing CheR from pZE21-CheR (grey) versus CW bias. The inset shows power spectral density as a function of noise frequency. Black line, power density averaged over all cells (wild-type RP437 and RP437 expressing CheR from pZE21-CheR) with CW bias = 0.15–0.20. Dark grey line, power density of the motor decoupled from the signalling network[3]. We determined the low-frequency noise for the region between the dotted lines. See Supplementary Fig. 5 for all CW bias bins. **b,** Signalling noise as a function of CW bias for wild-type RP437 cells and RP437 cells expressing CheR from pZE21-CheR. Signalling noise is defined as the variance $\sigma^2_{\text{CheY-P}}$ of the fluctuating [CheY-P]. Letters correspond to the CW bias bins (Fig. 1a). The power spectral densities and CW biases are averaged over cells within the same CW bias. Error bars show the standard error associated with the estimated signalling noise within each bin.

contribute to the observed output noise: the spontaneous noise associated with the signalling events of the chemotaxis network and the stochastic switching behaviour of the bacterial motor (Fig. 3a). The binary nature of the switching behaviour of the motor dominates the variance of the noise and masks the signalling noise within the chemotaxis network the output signalling molecule of which is the phosphorylated form of the signalling protein CheY[1,2]. The active form, CheY-P, binds to the sensory basal part of the flagella rotary motor and induces CW rotation. Using a procedure developed by ref. 22, we decoupled the signalling noise, $\sigma^2_{\text{CheY-P}}$, from that of the motor. We then found that the signalling noise decreased with the CW bias (Fig. 3b).

Operationally, we used a simplified expression of the FRT, in which the response function of the chemotaxis system $\mu(t)$ and the autocorrelation function $C(t)$ of the spontaneous fluctuations of the cellular behaviour should be related by $\mu(t) = -K\dfrac{\mathrm{d}}{\mathrm{d}t}C(t)$. Here, the fluctuation–response coupling coefficient K may depend on the genetic background,
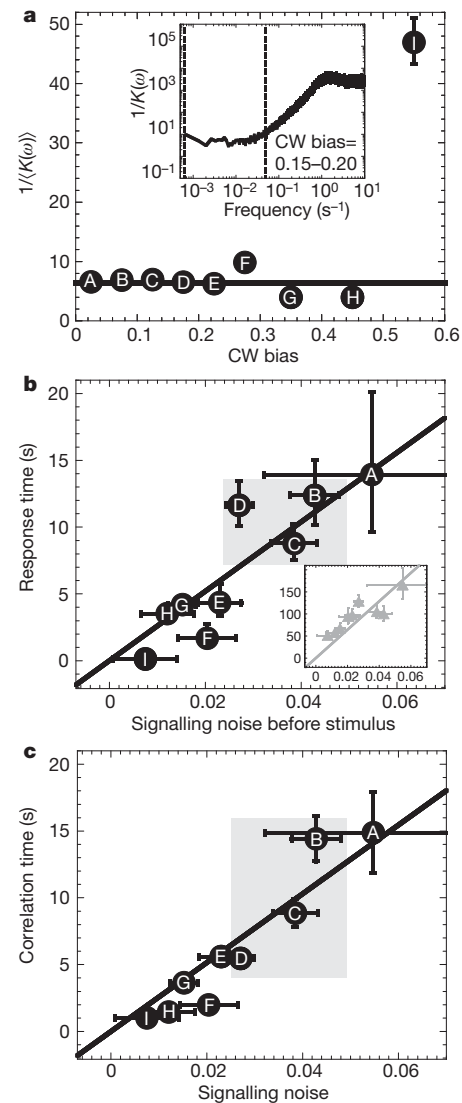

Figure 4 | Relationship between signalling noise and response time to a small external stimulus. a, Mean coupling coefficient $1/\langle K(\omega)\rangle_\omega$ for each CW bias bin. We computed the geometric mean over frequencies ranging from $1/1{,}500\,\mathrm{s}^{-1}$ to $1/20\,\mathrm{s}^{-1}$, represented by the dashed lines in the inset to **a.** We found that the coupling coefficient K for the small stimulus was constant at long timescales for frequencies in this range (see also Supplementary Fig. 7a). The standard error of the mean is smaller than the symbol size except for the highest CW bias bin I. The line is the mean value of $1/\langle K(\omega)\rangle_\omega$ computed over CW biases ranging from 0.00 to 0.5. The inset to **a** shows $1/K(\omega)$ for cells with a CW bias ranging from 0.15 to 0.20 (10 nM L-aspartate increase). For large stimulus K is not constant (see Supplementary Fig. 7b). **b,** Average response times of all cells (wild-type RP437 and RP437 expressing inducible CheR) to small stimulus (black circles) or large stimulus (grey triangles in inset to **b**) versus mean pre-stimulus signalling noise. Solid lines are linear fits forced through the origin. Response time $= C \times \sigma^2_{\text{CheY-P}}$. Black line: $C = 259 \pm 25\,\mathrm{s\,\mu M}^{-2}$ ($R^2 = 0.8$) for small stimulus. Grey line in inset to **b**: $C = 3{,}215 \pm 307\,\mathrm{s\,\mu M}^{-2}$ ($R^2 = 0.4$) for large stimulus. Grey area, representative behaviour of a wild-type population. The insets in **b** shares axes with the main panel. **c,** The correlation time as a function of the mean signalling noise before stimulus for all cells (wild-type RP437 and RP437 expressing CheR from pZE21-CheR). Black line, linear fit function forced through the origin. Correlation time $= C \times \sigma^2_{\text{CheY-P}}$. $C \approx 257 \pm 21\,\mathrm{s\,\mu M}^{-2}$ ($R^2 = 0.9$). Letters correspond to the CW bias bins (Fig. 1a). Error bars for the correlation time are the average half-lengths of the first uncorrelated CCW intervals. Error bars for the signalling noise are the standard error associated with the signalling noise in each bin. Grey area is representative behaviour of a wild-type population.

growth conditions, and functional state of the cell. We plotted the coefficient $K(\omega) = -\dfrac{2\,\mathrm{Im}[\tilde{\mu}(\omega)]}{\omega P(\omega)}$ as a function of CW bias, where $P(\omega)$ is the power spectral density of the spontaneous fluctuations (Fig. 4a and Supplementary Figs 6 and 7). In the most general non-equilibrium case, the coupling coefficient K may change when the genetic background or the growth conditions are modified. In chemotaxis, we found that the value of the coupling coefficient $K(\omega)$ is independent of the functioning states of the cell and levels of expression of the chemotaxis proteins (Fig. 4a). This result is remarkable because most of the chemotaxis network has highly nonlinear signal processing[23,24].

It is usual to consider that noise is an independent limiting factor in intracellular signalling and that evolution selects network designs to reduce it[25]. However, using the framework of the FRT, we asked whether the temporal fluctuations in the switching rate of the motor and the cellular response are ever dynamically coupled. Remarkably, we found that the response time to a small external stimulus scaled linearly with the signalling noise from the chemotaxis network in cells before stimulus ($R^2 = 0.8$; Fig. 4b), which was consequently linearly related to the correlation time ($R^2 = 0.9$; Fig. 4c). Furthermore, we found that the response time to a large stimulus scaled poorly ($R^2 = 0.4$) with the signalling noise, reflecting that for large stimulus, the system operates outside the regime of linear approximation (Fig. 4b, inset).

We interpret this observation in simple mathematical terms, where the fluctuations in the network output, $\delta_{\text{CheY-P}}$, about its average have linearized kinetics in the form of a Langevin equation[21,26]: $\dfrac{\mathrm{d}}{\mathrm{d}t}\delta_{\text{CheY-P}} = -\dfrac{1}{\tau}\delta_{\text{CheY-P}} + \sqrt{D}\delta\eta(t)$, where $\sqrt{D}\delta\eta(t)$ is a white-noise source with intensity D and τ is the measured correlation time in the output of the signalling system. In this coarse-grained picture, there should exist a strict relationship between the signalling output noise amplitude $\sigma^2_{\text{CheY-P}}$ and the time τ, where $\sigma^2_{\text{CheY-P}} = (D/2)\tau$. Although the coefficient D could potentially depend on intracellular parameters in a complex way, our experiments surprisingly showed that two cellular traits, $\sigma^2_{\text{CheY-P}}$ and the response time, are linearly coupled. This observation implies that the coefficient D remains approximately constant over a wide range of functioning states of the cell (that is, CW bias). This result is consistent with the fact that the coefficient $\langle K(\omega)\rangle_\omega$ (Fig. 4a) determines the behaviour of D, because $\langle K(\omega)\rangle_\omega \propto 1/D$. Consequently, we anticipate that below an upper bound imposed mainly by rotational diffusion[27], cells with the largest behavioural variability before stimulus would also exhibit the strongest chemotactic drift in response to an external stimulus[21].

Although the FRT predicts the existence of a coupling between cellular response and noise, it does not specify how this coupling depends on the different states of the cell. Therefore, we hypothesize that the specific design of the signalling pathways could govern such interdependence. We find that a simple kinetic model and experimental data support this hypothesis (Supplementary Fig. 8): in chemotaxis, the value of the coefficient D is governed by the adaptation mechanism that uses the classic futile cycle[21] as a core module in which two antagonistic enzymes regulate the activity of the kinase-receptor complexes. Because the futile cycle is a design shared by a large class of signalling pathways[21,28,29], it raises the possibility that for these systems, noise and cellular response are coupled in a similar way. To gain general insights into the selection of a specific coupling, we should examine how certain classes of design and function of networks may constrain the behaviour of this interdependence[30].

METHODS SUMMARY

Response time. For each cell (whose behaviour is defined by a specific CW bias bin), the response time was measured from the time of stimulus through all successive averaged CCW intervals that were longer than the mean pre-stimulus CCW interval length. This mean was obtained by averaging together the CCW

interval lengths chosen at random time points within the binary time series of the non-stimulated cell.

Correlation time. To determine the correlation time of the CCW sequences, we used serial correlation coefficients (Supplementary Fig. 4c) for the CCW interval lengths[19,20]. We converted the correlated number of sequences to the real correlation time lengths, including the half-length of the first uncorrelated CCW interval. To determine whether the sequences in each lag (the number of preceding CCW intervals) were correlated, we used the Wilcoxon rank sum test (the "ranksum" Matlab function) at a significance level of $P = 0.01$ (Supplementary Fig. 4d), as in ref. 20. We considered the first non-zero lag that had $h = 0$ as the end of the correlation.

Low-frequency noise and motor noise. We define the low-frequency noise N_i^{LF} of the ith cell as the integrated power density $P_i(f)$ of the binary time series from $f_i = 1/1{,}500\,\mathrm{s}^{-1}$ to $f_f = 1/10\,\mathrm{s}^{-1}$, which is $N_i^{\text{LF}} \equiv \displaystyle\int_{f_i}^{f_f} P_i(f)\mathrm{d}f$ (Fig. 3a). We define the low-frequency motor noise $N_i^{\text{LF,M}}$ as the integrated flat baseline of the power density (Fig. 3a, dark grey line) on the same timescale. We estimated signalling noise from the average experimental power spectral density, the average CW bias, and the gain function between the input signal (steady-state [CheY-P]) and output signal (average CW bias) using methods introduced by ref. 22 (Methods).

Full Methods and any associated references are available in the online version of the paper at www.nature.com/nature.

1. Bourret, R. B., Borkovich, K. A. & Simon, M. I. Signal transduction pathways involving protein phosphorylation in prokaryotes. *Annu. Rev. Biochem.* **60**, 401–441 (1991).
2. Bourret, R. B. & Stock, A. M. Molecular information processing: lessons from bacterial chemotaxis. *J. Biol. Chem.* **277**, 9625–9628 (2002).
3. Korobkova, E. A., Emonet, T., Park, H. & Cluzel, P. Hidden stochastic nature of a single bacterial motor. *Phys. Rev. Lett.* **96**, 058105 (2006).
4. Callen, H. B. & Welton, T. A. Irreversibility and generalized noise. *Phys. Rev.* **83**, 34–40 (1951).
5. Prost, J., Joanny, J. F. & Parrondo, J. M. Generalized fluctuation-dissipation theorem for steady-state systems. *Phys. Rev. Lett.* **103**, 090601 (2009).
6. Bustamante, C., Macosko, J. C. & Wuite, G. J. L. Grabbing the cat by the tail: manipulating molecules one by one. *Nature Rev. Mol. Cell Biol.* **1**, 130–136 (2000).
7. Dorignac, J., Kalinowski, A., Erramilli, S. & Mohanty, P. Dynamical response of nanomechanical oscillators in immiscible viscous fluid for *in vitro* biomolecular recognition. *Phys. Rev. Lett.* **96**, 186105 (2006).
8. Paulsson, J. Summing up the noise in gene networks. *Nature* **427**, 415–418 (2004).
9. Ozbudak, E. M., Thattai, M., Kurtser, I., Grossman, A. D. & van Oudenaarden, A. Regulation of noise in the expression of a single gene. *Nature Genet.* **31**, 69–73 (2002).
10. Cugliandolo, L. F., Dean, D. S. & Kurchan, J. Fluctuation-dissipation theorems and entropy production in relaxational systems. *Phys. Rev. Lett.* **79**, 2168–2171 (1997).
11. Chetrite, R., Falkovich, G. & Gawedzki, K. Fluctuation relations in simple examples of non-equilibrium steady states. *J. Stat. Mech.-Theory E* **2008**, P08005 (2008).
12. Speck, T. & Seifert, U. Restoring a fluctuation-dissipation theorem in a nonequilibrium steady state. *Europhys. Lett.* **74**, 391–396 (2006).
13. Berg, H. C. Motile behavior of bacteria. *Phys. Today* **53**, 24–29 (2000).
14. Korobkova, E., Emonet, T., Vilar, J. M., Shimizu, T. S. & Cluzel, P. From molecular noise to behavioural variability in a single bacterium. *Nature* **428**, 574–578 (2004).
15. Cluzel, P., Surette, M. & Leibler, S. An ultrasensitive bacterial motor revealed by monitoring signaling proteins in single cells. *Science* **287**, 1652–1655 (2000).
16. Sourjik, V. & Berg, H. C. Receptor sensitivity in bacterial chemotaxis. *Proc. Natl Acad. Sci. USA* **99**, 123–127 (2002).
17. Barkai, N. & Leibler, S. Robustness in simple biochemical networks. *Nature* **387**, 913–917 (1997).
18. Alon, U., Surette, M. G., Barkai, N. & Leibler, S. Robustness in bacterial chemotaxis. *Nature* **397**, 168–171 (1999).
19. Anderson, R. L. Distribution of the serial correlation coefficient. *Ann. Math. Stat.* **13**, 1–13 (1942).
20. Ratnam, R. & Nelson, M. E. Nonrenewal statistics of electrosensory afferent spike trains: implications for the detection of weak sensory signals. *J. Neurosci.* **20**, 6672–6683 (2000).
21. Emonet, T. & Cluzel, P. Relationship between cellular response and behavioral variability in bacterial chemotaxis. *Proc. Natl Acad. Sci. USA* **105**, 3304–3309 (2008).
22. Shibata, T. & Fujimoto, K. Noisy signal amplification in ultrasensitive signal transduction. *Proc. Natl Acad. Sci. USA* **102**, 331–336 (2005).
23. Bray, D., Levin, M. D. & Morton-Firth, C. J. Receptor clustering as a cellular mechanism to control sensitivity. *Nature* **393**, 85–88 (1998).
24. Sourjik, V. & Berg, H. C. Functional interactions between receptors in bacterial chemotaxis. *Nature* **428**, 437–441 (2004).
25. Rao, C. V., Wolf, D. M. & Arkin, A. P. Control, exploitation and tolerance of intracellular noise. *Nature* **420**, 231–237 (2002).

26. Bialek, W. & Setayeshgar, S. Physical limits to biochemical signaling. *Proc. Natl Acad. Sci. USA* **102,** 10040–10045 (2005).
27. Andrews, B. W., Yi, T. M. & Iglesias, P. A. Optimal noise filtering in the chemotactic response of *Escherichia coli. PLOS Comput. Biol.* **2,** e154 (2006).
28. Goldbeter, A. & Koshland, D. E. Jr. An amplified sensitivity arising from covalent modification in biological systems. *Proc. Natl Acad. Sci. USA* **78,** 6840–6844 (1981).
29. Detwiler, P. B., Ramanathan, S., Sengupta, A. & Shraiman, B. I. Engineering aspects of enzymatic signal transduction: photoreceptors in the retina. *Biophys. J.* **79,** 2801–2817 (2000).
30. Shinar, G. & Feinberg, M. Structural sources of robustness in biochemical reaction networks. *Science* **327,** 1389–1391 (2010).

Author Contributions P.C. conceived and designed the research. H.P. performed all the experiments. H.P., P.C., T.E., W.P. and J.F.M. analysed the data. H.P., P.C., J.F.M. and T.E. wrote the paper. C.C.G. constructed the pZE21-CheR plasmid.

Author Information Reprints and permissions information is available at www.nature.com/reprints. The authors declare no competing financial interests. Readers are welcome to comment on the online version of this article at www.nature.com/nature. Correspondence and requests for materials should be addressed to P.C. (cluzel@mcb.harvard.edu).

METHODS

Strains and plasmids. RP437 is a wild-type *E. coli* strain for chemotaxis[31]. To construct pZE21-CheR, we amplified *cheR* using polymerase chain reaction (PCR) from the chromosome of the RP437 strain with the following primers: CheR-KpnI-5′: 5′-gcc ggt acc atg act tca tca tct ctg ccc tg-3′ and CheR-HindIII-3′: 5′-cgc aag ctt tta atc ctt act tag cgc at-3′. The gene fragment was inserted in the KpnI and HindIII sites of a pZE21 series plasmid[30] that contained a kanamycin resistance cassette and a TetR inducible promoter. The plasmid pZS4-Int1 encodes *tetR* under a constitutive promoter, which modulates the expression of the TetR-regulated *cheR* construct[32]. This plasmid carries a spectinomycin resistance gene. Wild-type cells with and without plasmid exhibited similar noise levels (Fig. 3a) and CCW interval lengths after stimulus (Supplementary Fig. 1a, c and d) at the single-cell level.

HPLC calibration of the release of aspartate. We prepared 10 μl samples of 0.5-mM caged L-aspartate solution under the same conditions for the chemotaxis experiments and illuminated them with intense ultraviolet light from a Xenon flash lamp (built-in L7685 reflective mirror, 60 W, Hamamatsu). We estimated the relative concentration of the caged L-aspartate in each sample by the high-performance liquid chromatography (HPLC) peak area. By comparing the decreasing HPLC peak area with its initial peak area, we found the released L-aspartate concentration as a function of the number of ultraviolet flashes (Supplementary Fig. 9). The samples released about 1 μM L-aspartate per ultraviolet flash. The HPLC gradient conditions had five steps: (1) equilibrium with 20% acetonitrile, 0.1% TFA/80% water, 0.1% TFA; (2) gradient of 20–55% acetonitrile over 30 min; (3) first washing with 55–90% acetonitrile for 20 min; (4) second washing with 90% acetonitrile for 5 min; and (5) equilibrium with 20% acetonitrile, 0.1% TFA/80% water, 0.1% TFA.

Photo-release and single-cell assay. We sheared the flagella of the cells by slowly forcing them through a thin needle (inner diameter = 0.19 mm, 27 G ½, B-D) 40 times. Cultures grew overnight in 3 ml of tryptone broth at 35 °C with shaking at 200 r.p.m. We transferred the overnight cultures to a 250 ml flask, in which we diluted them 1:50 in 12-ml tryptone broth and grew the cells again at 35 °C at 200 r.p.m. To obtain cells with different CW biases, we induced plasmid expression with various concentrations of anhydrotetracycline (0–2.5 ng ml⁻¹) in the diluted overnight cultures. The media also contained the antibiotic specific for the plasmid. We harvested the cells when the absorbance A reached ~0.3 at 600 nm. We washed the cells and resuspended them in motility medium (0.1 mM EDTA, 0.1 mM L-methionine, 10 mM potassium phosphate pH 7.0). We prepared glass slides (No. 1½, 18 mm, Corning) coated with poly-L-lysine and a solution of beads (Polybead Amino 1.0 μm Microspheres, Polysciences) coated with rabbit antibodies against flagella. We mixed the cells (4–5 μl) with the beads (4–5 μl) and incubated them for 20 min at room temperature (21–22 °C). This process caused the cell bodies to stick to the glass slide and the beads to attach to the flagella. Although the probability of a bead attaching to a rotating flagellum was low, we consistently obtained a few labelled flagella in each sample. After incubation we removed the unattached cells and beads and then added 8 μl of 5 μM (for small stimulus) or 500 μM (for large stimulus) caged L-aspartate solution to the sample medium. We covered the sample with oil (immersion oil transparent to ultraviolet: type FF, Cargille Laboratories) to prevent evaporation. We placed the sample under a dark-field condenser to produce a bright red image of the bead. Harmful blue light was filtered out by a long-pass filter (NT52-543, Edmund Industrial). We observed the samples under an Olympus IX71 microscope with an oil immersion objective 100× (numerical aperture = 1.3, Olympus Uplan FI, oil iris ∞/0.17). We recorded the long circular motions of individual beads attached to rotating flagella of single cells through a four-quadrant photomultiplier (type: R5900U-01-M4, Hamamatsu). The signal from the photomultiplier, a four-voltage time series, was monitored with a PC computer via LabView software (National Instrument). The rotation of the bead was simultaneously recorded using a charge-coupled device camera (1/3′′ midresolution Exview digital B/W camera, Sony). We converted the signal to a binary time series indicating transitions between CCW and CW rotations. After 1,500 s (or 300 s) of recording the rotational motion of the bead, we photo-released the caged aspartate (caged l-aspartic acid, sodium salt (189110): *N*-[1-(2-nitrophenyl)ethyloxycarbonyl]aspartic acid, sodium, $C_{13}H_{13}N_2O_8$·Na, relative molecular mass 348.2 and molar absorption ε = 4,710 M⁻¹ cm⁻¹ at maximum wavelength $λ_{max}$ = 264 nm), from Calbiochem or synthesized by D. Trentham, G. Reid and J. Corrie. We illuminated the sample with an intense ultraviolet light from the Xenon flash coupled into a light guide (A2873, quartz glass fibre, Hamamatsu) and widely focused onto the whole sample with two ultraviolet-coated lenses (focal length = 35 mm and diameter = 25.4 mm; focal length = 20 mm and diameter = 12.7 mm, ThorLabs). These ultraviolet flashes produced a stepwise release of 1 μM (or 10 nM) L-aspartate from the 0.5 mM (or 5 μM) caged L-aspartate[33]. The magnitude of the stepwise stimulus corresponds to the typical increase in attractant concentration encountered by bacteria swimming in a gradient of 1 nM μm⁻¹ (refs 34 and 35).

Definition of CW bias. We define $T_{i,j}^{CW}$ and $T_{i,j}^{CCW}$ as the durations of the jth CW and CCW intervals of the ith cell. The CW bias for the jth CW-to-CCW interval pair of the ith cell is $b_{i,j} = T_{i,j}^{CW} / \left(T_{i,j}^{CCW} + T_{i,j}^{CW} \right)$. The pre-stimulus CW bias of the ith cell, $\left\langle b_{i,j} \right\rangle_{before}$, is the time average of $b_{i,j}$ over a time window of length $t_{i,before}$ preceding the stimulus. $t_{i, before}$ was 300 s for the cells with CW bias exceeding 0.25 responding to the large stimulus and 1,500 s for all other cells. Similarly, the post-stimulus CW bias of the ith cell, $\left\langle b_{i,j} \right\rangle_{after}$, is the temporal average of $b_{i,j}$ over a time window of duration $t_{i, after}$ seconds following the stimulus. For the small (or large) stimulus, the first two (or 200) CW–CCW interval pairs following stimulus were not included. $t_{i, after}$ was 1,500 s for small stimuli, 900 s for large stimuli and CW bias <0.25, and 300 s for large stimuli and CW bias >0.25.

Response time. For each cell (the behaviour of which is defined by a specific CW bias bin), the response time was measured from the time of stimulus through all successive averaged CCW intervals that were longer than the mean pre-stimulus CCW interval length. This mean was obtained by averaging together the CCW interval lengths chosen at random time points within the binary time series of the non-stimulated cell. If the response time included more than one CCW interval, the CW interval length between two successive CCW intervals was also included in the response time. To get the final response time, we subtracted the mean non-stimulated portion of the first responding CCW interval. For example, if the third CCW interval is the last CCW interval length significantly longer than the mean CCW interval length before stimulus (dashed line in Figs 1b and c), the response time would be:

$$\langle T_{CCW, 1st} \rangle + \langle T_{CW, 1st} \rangle + \langle T_{CCW, 2nd} \rangle + \langle T_{CW, 2nd} \rangle +$$
$$\langle T_{CCW, 3rd} \rangle - \langle T_{CCW, 1st, prestimulus} \rangle$$

The dashed line in Fig. 1b and c and Supplementary Fig. 1e represents the trend of the mean pre-stimulus CCW interval length in each CW bias bin. Because of the presence of a few outliers, we used the geometric mean to compute the trend of the mean CCW interval lengths after stimulus and mean pre-stimulus CCW interval length within each CW bias bin (Fig. 1b and c).

Correlation time. To determine the correlation time of the CCW sequences, we used serial correlation coefficients (Supplementary Fig. 4c) for the CCW interval lengths[19,20]. We converted the correlated number of sequences to the real correlation time lengths, including the half-length of the first uncorrelated CCW interval. To determine whether the sequences in each lag (the number of preceding CCW intervals) were correlated, we used the Wilcoxon rank sum test (the "ranksum" Matlab function) at a significance level of $P = 0.01$ (Supplementary Fig. 4d) as in ref. 20. We considered the first non-zero lag that had $h = 0$ as the end of the correlation.

Low-frequency noise and motor noise. We define the low frequency noise N_i^{LF} of the ith cell as the integrated power density $P_i(f)$ of the binary time series from $f_i = 1/1,500\ s^{-1}$ to $f_f = 1/10\ s^{-1}$, which is $N_i^{LF} \equiv \int_{f_i}^{f_f} P_i(f)\mathrm{d}f$ (Fig. 3a). We define the low-frequency motor noise $N_i^{LF,M}$ as the integrated flat baseline of the power density (Fig. 3a, dark grey line) on the same timescale.

Estimating signalling noise. To estimate the signalling noise, we used a formula $\sigma_{M, total}^2 \cong \sigma_M^2 + g_M^2 \overline{b}^2 \frac{\sigma_{CheY-P}^2}{[CheY-P]^2}$ which shows the relationship between the variance σ_{CheY-P}^2 of [CheY-P] and the variance $\sigma_{M, total}^2$ of the output signals. This formula was derived from a model recently introduced to describe generally the gain–noise relationship between the input and output signals in the chemical reaction network[22]. As ref. 22 showed, the temporally fluctuating output signal from a well defined steady state (CW bias = $\overline{b}$) due to the fluctuating input signal ([CheY-P]) is described by the following linearized chemical Langevin equation: $\dot{\delta b} = \gamma_M \delta[CheY-P] - \delta b/\tau_M + \xi_M(t)$, where δb and $\delta[CheY-P]$ are small deviations of the CW bias and [CheY-P] from their steady values, respectively, τ_M is the typical timescale of the motor alone and $\xi_M(t)$ is the Gaussian white-noise term that satisfies $\overline{\xi_M(t)} = 0$ and $\overline{\xi_M(t)\xi_M(t')} = \sigma_{\xi_M}^2 \cdot \delta(t-t')$. From this equation, we obtain the total variance of the output signals due to the temporally fluctuating input signals and the Gaussian white noise:

$$\sigma_{M, total}^2 = \frac{g_M \overline{b}}{\Theta_M} + g_M^2 \overline{b}^2 \frac{\tau_{CheY-P}}{\tau_M + \tau_{CheY-P}} \frac{\sigma_{CheY-P}^2}{[CheY-P]^2}$$

where $\overline{[CheY-P]}$ is the steady value of fluctuating [CheY-P] values given by:

$$\overline{[CheY-P]} = K_M \left(\frac{\overline{b}}{1-\overline{b}} \right)^{1/N_H}$$

where K_M (half the concentration of CheY-P that yields CW bias = 0.5) and the Hill coefficient N_H are given by 3.1 µM and 10.3, respectively, in ref. 15). The constant Θ_M in the first term is defined by $\Theta_M \equiv 2\gamma_M \overline{[\text{CheY-P}]}\big/\sigma_{\xi_M}^2$ and $\overline{b}$ is the CW bias. g_M is the gain function defined as the ratio of the fractional change of the output signal to the input signal: that is, $g_M = \left(\delta b/\overline{b}\right)\big/$ $\left(\delta[\text{CheY-P}]/\overline{[\text{CheY-P}]}\right) = N_H\left(1-\overline{b}\right)$, where $N_H\left(1-\overline{b}\right)$ is obtained from ref. 15. $\tau_{\text{CheY-P}}$ is a characteristic timescale of the [CheY-P] fluctuations and is proportional to the input noise $\sigma_{\text{CheY-P}}^2$ as follows: $\tau_{\text{CheY-P}} = \dfrac{\sigma_{\xi_{\text{CheY-P}}}^2}{2}\sigma_{\text{CheY-P}}^2$. This relationship is derived from the chemical Langevin equation describing the [CheY-P] fluctuations from its steady state ($\overline{[\text{CheY-P}]}$):

$$\dot{\delta[\text{CheY-P}]} = -\frac{\delta[\text{CheY-P}]}{\tau_{\text{CheY-P}}} + \xi_{\text{CheY-P}}(t)$$

where $\xi_{\text{CheY-P}}(t)$ is a Gaussian white-noise term that satisfies $\overline{\xi_{\text{CheY-P}}(t)} = 0$ and $\overline{\xi_{\text{CheY-P}}(t)\cdot\xi_{\text{CheY-P}}(t')} = \sigma_{\xi_{\text{CheY-P}}}^2 \cdot \delta(t-t')$. As long as the external stimulus is small enough, the response time to the stimulus should scale to $\tau_{\text{CheY-P}}$. For the broad range of the functioning states of this paper, we have one condition, $\tau_{\text{CheY-P}} \gg \tau_M$, in the timescales involved in this system. Under this condition, the above formula for the total variance of the output signals can be simplified to

$$\sigma_{\text{M, total}}^2 \cong \sigma_M^2 + g_M^2\overline{b}^2\frac{\sigma_{\text{CheY-P}}^2}{\overline{[\text{CheY-P}]}^2}$$

where $\sigma_{\text{M, total}}^2$ is given by $\overline{b}\left(1-\overline{b}\right)$ for any binary time series and is equal to the integral of the power spectral density over all frequencies (black line in Supplementary Fig. 5) averaged over all cells (wild-type RP437 and RP437 expressing CheR from pZE21-CheR) and σ_M^2 is equal to the integral of the power density (dark grey line in Supplementary Fig. 5) of the isolated motor. We approximated the baseline of the motor power density by finding the mean value of the flat regime (from $f_i = 1/10\,\text{s}^{-1}$ to $f_f = 1/5\,\text{s}^{-1}$) of the average experimental power density and extending the baseline to the lowest frequency. By using the simplified formula above, we estimated the $\sigma_{\text{CheY-P}}^2$ values in each CW bias bin (Fig. 3b).

Definition of noise. We hypothesize that a small number of proteins and thermally activated biochemical reaction rates cause stochastic fluctuations between functional states of signalling proteins. Operationally, we monitor the cellular behaviour in a motility medium that does not support growth but allows bacteria to perform chemotaxis. Under these conditions, the observed noise does not result from protein synthesis or degradation; rather, it results from fluctuations in protein functional states about a well-defined steady state.

31. Parkinson, J. S. & Houts, S. E. Isolation and behavior of *Escherichia coli* deletion mutants lacking chemotaxis functions. *J. Bacteriol.* **151,** 106–113 (1982).
32. Lutz, R. & Bujard, H. Independent and tight regulation of transcriptional units in *Escherichia coli* via the LacR/O, the TetR/O and AraC/I1-I2 regulatory elements. *Nucleic Acids Res.* **25,** 1203–1210 (1997).
33. Jasuja, R., Yu-Lin, Trentham, D. R. & Khan, S. Response tuning in bacterial chemotaxis. *Proc. Natl Acad. Sci. USA* **96,** 11346–11351 (1999).
34. Adler, J. A method for measuring chemotaxis and use of the method to determine optimum conditions for chemotaxis by *Escherichia coli*. *J. Gen. Microbiol.* **74,** 77–91 (1973).
35. Bainer, R., Park, H. & Cluzel, P. A high-throughput capillary assay for bacterial chemotaxis. *J. Microbiol. Methods* **55,** 315–319 (2003).